Methane to Methanol Transformation on Cu^{2+}/H-ZSM-5 Zeolite. Characterization of Copper State and Mechanism of the Reaction

Gabrienko, Anton A.; Kolganov, Alexander A.; Yashnik, Svetlana A.; Kriventsov, Vladimir V.; Stepanov, Alexander G.

DOI
10.1002/chem.202403167

Publication date
2025

Document Version
Final published version

Published in
Chemistry - A European Journal

Chemistry–A European Journal
Research Article
doi.org/10.1002/chem.202403167
Chemistry Europe
European Chemical Societies Publishing
www.chemeurj.org

Methane to Methanol Transformation on Cu^{2+}/H-ZSM-5 Zeolite. Characterization of Copper State and Mechanism of the Reaction

Anton A. Gabrienko,*[a] Alexander A. Kolganov,[a] Svetlana A. Yashnik,[a] Vladimir V. Kriventsov,[b] and Alexander G. Stepanov*[a]

Cu-modified zeolites provide methane conversion to methanol with high selectivity under mild conditions. The activity of different Cu-sites for methane transformation is still under discussion. Herein, ZSM-5 zeolite has been loaded with Cu^{2+} cations (1.4 wt% Cu) as characterized by UV-vis DRS, EPR, EXAFS, and ^{1}H MAS NMR. It is inferred that Cu^{2+} cations, attached to the cation-exchange Al–O^{-}–Si sites of the zeolite framework, can exist in the form of either isolated or paired Cu^{2+} sites. The transformation of methane to methanol on Cu^{2+}/H-ZSM-5 has been verified by the observation of the methoxy species formation with ^{13}C MAS NMR and FTIR spectroscopy. The related mechanisms have been analyzed by DFT calculations. The calculations show that the paired Cu^{2+} sites enable heterolytic C–H bond dissociation via the "alkyl" pathway resulting in methylcopper species, which however are not detected experimentally due to further rapid transformation to surface methoxy species through methyl radical formation and recombination with Si–O^{-}Al site. Based on the obtained data, it has been concluded that methane transformation to methanol on paired Cu^{2+} sites, having no extra-framework oxygen ligand, is possible in Cu-modified zeolites. The pathways of Cu^{2+} cations regeneration with O_2 and H_2O have been experimentally explored.

Introduction

Methane, being a widely accessible raw material,[1] has great potential as an inexpensive reactant for the chemical industry.[2] The selective low-temperature conversion of methane to valuable chemicals such as methanol,[3] acetic acid,[4] and aromatic compounds[5] on metal-modified zeolites and metal oxides is considered to be a promising alternative to high-temperature and energy-consuming processes of methane utilization via intermediate syngas production.[2] The search for the optimal catalytic processes for rational methane conversion is currently a focus of research groups worldwide.

Cu-modified zeolites are considered to be promising catalysts for methane utilization.[6] Methane chemical activation by these catalysts was reported in the pioneering work by Groothaert et al.[6a] That study of Cu-containing ZSM-5, MOR, and other zeolites was inspired by the properties of methane monooxygenase (MMO) that contains some copper-oxo active sites capable of converting methane into methanol at ambient temperature and pressure with almost 100% selectivity.[7] Importantly, extra-framework copper species of great diversity, such as Cu^{2+} cations,[8] multinuclear copper-oxo clusters,[9] linear CuO-like chains,[10] could be loaded in the zeolite pores by the post-synthetic modification. To date, the following copper species of different compositions and structures possessing activity for methane transformation were identified: mononuclear $[Cu^{2+}–OH]^{+}$, $[Cu^{2+}O]^{+}$, and Cu^{2+} cationic species,[6f,m,11] binuclear $[Cu_2(\mu\text{-}O)]^{2+}$ [6b] and trinuclear $[Cu_3(\mu\text{-}O)_3]^{2+}$ oxo-clusters.[6c,e,g,11] The reactivity of the trinuclear copper-oxo clusters is currently under intense investigation.[6j,12] It is considered that the extra-framework O-ligands are crucial for the reactivity of copper-oxo clusters.[6c,e,f,13] On the other hand, the possibility of methane activation by Cu^{2+} cations[6l–n] has not been fully understood so far.

In this work, a Cu-containing H-ZSM-5 zeolite sample, selectively modified with Cu^{2+} cations, was intentionally prepared. The state of the copper sites was analyzed by EXAFS, UV-vis DRS, and EPR methods and it was shown that copper species in the zeolite were mainly represented by isolated or paired Cu^{2+} sites bound to the framework cation-exchange Si–O^{-}–Al sites. ^{13}C MAS NMR and FTIR spectroscopy study has shown the formation of methoxy species and methanol from methane on this zeolite sample. The mechanism of methane transformation to methanol involving cationic Cu^{2+} sites was analyzed by DFT calculations. Additionally, the possible pathways of Cu^{2+} cations regeneration by O_2 or H_2O were explored experimentally.

[a] A. A. Gabrienko, A. A. Kolganov, S. A. Yashnik, A. G. Stepanov
Boreskov Institute of Catalysis, Siberian Branch of the Russian Academy of Sciences, Prospekt Akademika Lavrentieva 5, Novosibirsk 630090 Russia
and
Dr. A. A. Kolganov current address: Inorganic Systems Engineering (ISE), Department of Chemical Engineering, Delft University of Technology, 2629 HZ Delft, The Netherlands
E-mail: stepanov@catalysis.ru
gabrienko@catalysis.ru

[b] V. V. Kriventsov
Synchrotron Radiation Facility SKIF, Boreskov Institute of Catalysis, Kol'tsovo 630559, Russia

Supporting information for this article is available on the WWW under https://doi.org/10.1002/chem.202403167

Results and Discussion

Characterization of Copper Sites in Cu-Modified ZSM-5 Zeolite

EXAFS Data

The curves of the radial distribution function (RDF), describing the Cu atom local arrangement and resulting from the EXAFS spectra of the zeolite samples and reference materials, are presented in Figure 1. The structural parameters, such as interatomic Cu–O and Cu–O–Cu distances (R) and Cu coordination number (CN), derived from the EXAFS data, are shown in Table 1 for the Cu^{2+}/H-ZSM-5 sample and in Table S1 for bulk CuO and Cu-foil.

The RDF curve of Cu-foil (Figure 1a) shows peaks related only to the Cu–Cu distances of metallic copper. The main peak, located in the region of 1.65–2.86 Å, corresponds to the shortest Cu–Cu distances in the FCC metal structure.[14] RDF curve fitting gives the structural parameters R_{Cu-Cu} = 2.54 Å and CN = 12.0 for the main peak (Table S1). Other observed peaks are attributed to the next Cu–Cu distances. Considering this data, no metallic form of Cu^0 was found in Cu^{2+}/H-ZSM-5 within the sensitivity of the EXAFS method. This is also confirmed by the observation of only cationic copper species in the X-ray photoelectron spectra of the activated Cu^{2+}/H-ZSM-5 (Figure S1).

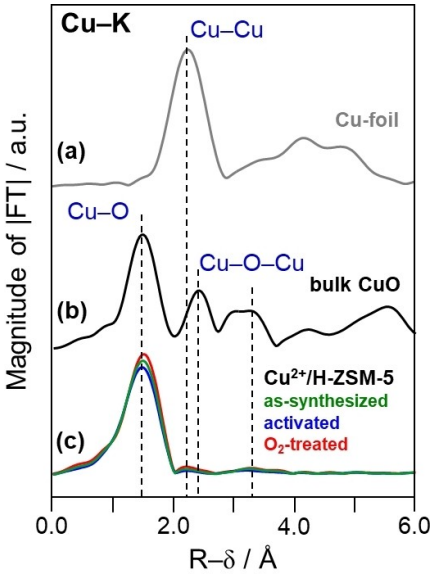

Figure 1. Radial distribution function (RDF) curves describing Cu local arrangement for the reference samples, Cu-foil (a) and bulk CuO (b), and Cu^{2+}/H-ZSM-5 (c). For the zeolite, RDF curves are presented for the following samples: as-synthesized (green line), after vacuum activation at 673 K (blue line), and further treated with O_2 at 673 K (red line).

Table 1. EXAFS structural parameters for Cu species in Cu^{2+}/H-ZSM-5 zeolite samples, Cu–O distance (R_{Cu-O}) and Cu coordination number (CN).

Sample	RCu–O/Å	CN
as-synthesized	1.94	4.3
activated	1.94	4.1
O_2-treated	1.95	4.5

The RDF curve of bulk CuO (Figure 1b) has characteristic peaks distinct from those for metallic copper. The first intense peak in the region of 1.3–2.2 Å is assigned to the shortest Cu–O distances typical of CuO_4 arrangement.[15] The parameters obtained by RDF curve fitting (Table S1) are R_{Cu-O} = 1.96 Å, CN = 4.1. The next peaks are those from the other distances, for instance, Cu–O–Cu, typical of bulk CuO.[15]

The RDF curves for the Cu^{2+}/H-ZSM-5 sample are shown in Figure 1c. The curves show the main peak at 1.0–2.1 Å, which is attributed to the nearest Cu–O distance after the comparison with the CuO reference. Importantly, no peaks were found in the region of 2–4 Å, unlike those for bulk CuO or Cu-modified MOR and ZSM-5 zeolites containing $[Cu_3(\mu\text{-}O)_3]^{2+}$ species.[6c,16] Hence, the formation of a noticeable number of copper-oxo clusters or large CuO-like agglomerates can be excluded, at least within the sensitivity of the EXAFS method. This is also confirmed by XRD and TEM methods (Figure S2). In particular, the X-ray diffractogram of as-synthesized Cu^{2+}/H-ZSM-5 exhibits only the reflections related to the MFI-type zeolite phase (Figure S2a).[17] TEM images demonstrate the uniform spatial distribution of Si, Al, and Cu atoms over the intracrystalline zeolite void and the absence of any copper agglomerates on the external surface of the zeolite crystals (Figure S2b). Therefore, the obtained RDF curves are due to the contribution of Cu^{2+} cations attached to the framework Si–O^-–Al sites of the zeolite. The structural parameters obtained after curve fitting are shown in Table 1 and are similar to those previously reported for ZSM-5 and MOR zeolites containing Cu^{2+} cationic sites[18]: R_{Cu-O} = 1.94–1.95 Å and CN = 4.1–4.5. It should be noted the CN value obtained for the studied samples is lower than that observed by UV-Vis DRS and EPR methods (*vide infra*). This is likely caused by the low sensitivity of the EXAFS method towards the ligands located in the first coordination sphere but at different distances from Cu^{2+} cation, similar to the case with $[Cu(H_2O)_6]^{2+}$ complexes whose geometry is distorted due to the Jahn-Teller effect.[19]

Different treatments of Cu^{2+}/H-ZSM-5 do not affect the position and the number of the detected peaks (Figure 1c). This means that the structure and composition of the major part of the copper species present in the zeolite sample are intact. However, it can be seen that the vacuum activation of the sample (at 673 K) leads to a slight reduction in the amplitude of the main Cu–O peak and related CN of copper atoms, as compared to the parameters of the as-synthesized sample (Table 1). Such changes can indicate the reduction of a minor portion of Cu^{2+} sites to Cu^+ ones and a decrease in the number of O-ligands.[18] If the activated sample was treated with O_2, the intensity of the peak and coordination number increased. Hence, the treatment of the activated sample with O_2 leads to the reverse oxidation of Cu^+ to Cu^{2+} and an increase in the number of O-ligands in the first coordination sphere of the copper atoms.

UV-Vis DRS Data

The spectrum of the as-synthesized Cu^{2+}/H-ZSM-5 sample (Figure 2, line 1) shows two bands at 12300 and 47500 cm^{-1}. These bands are assigned to the d-d transition of Cu^{2+} and the O^{2-}–Cu^{2+} ligand-to-metal charge transfer (LMCT) bands of $[Cu(H_2O)_6]^{2+}$ cations, respectively.[20] Another absorbance at >38000 cm^{-1} is accounted for by the fundamental absorption edge of ZSM-5 zeolite (Figure S3).[21] Importantly, the specific bands related to the agglomerated copper species are absent in the spectrum of Cu^{2+}/H-ZSM-5.

The activated Cu^{2+}/H-ZSM-5 sample (Figure 2, line 2) exhibits two main bands at 44200 cm^{-1} (O^{2-}–Cu^{2+} LMCT) and 13900 cm^{-1} (Cu^{2+} d-d transition) indicating the presence of Cu^{2+} cations in the O-environment.[6m,9b,18a,22] The shift, broadening, and increased intensity of the detected bands, as compared to the as-synthesized sample, indicate water molecules removal from the coordination sphere of Cu^{2+} cations and the strong interaction of Cu^{2+} with the framework Si–O^-Al sites. According to the energy of the observed bands, these cations have D_{4h} and C_{4v} symmetry of the O-ligand field. Additionally, the spectrum of activated zeolite demonstrates an absorbance at 17700–25000 cm^{-1} which is assigned[21] to the intervalence transition related to the presence of Cu^+ species, usually appearing after high-temperature dehydration of Cu-modified zeolites.[18a,21,23]

The treatment of the Cu^{2+}/H-ZSM-5 sample with O_2 leads to the following changes in the spectra (Figure 2, line 3). The intensities of the LMCT and d-d transition bands slightly increase and broad absorption from Cu^+ species (intervalence transitions) disappears. This indicates Cu^+ oxidation to Cu^{2+}. This is accompanied by the appearance of a new O^{2-}–Cu^{2+} LMCT band at 32000 cm^{-1} which indicates the formation of extra-framework CuO-like species[6c] presumably as $[Cu_3(\mu\text{-}O)_3]^{2+}$ oxo-clusters.[6c,e]

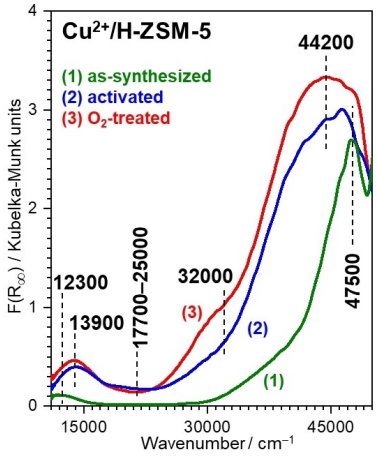

Figure 2. UV-vis DR spectra of Cu^{2+}/H-ZSM-5 samples: as-synthesized (green line, 1), after vacuum activation at 673 K (blue line, 2), and further treated with O_2 at 673 K (red line, 3).

EPR Data

The EPR spectra of Cu^{2+}/H-ZSM-5 samples are presented in Figure 3. The as-synthesized sample exhibits a signal with $g_{||} = 2.38$ and $g_{\perp} = 2.07$ which is typical of hydrated Cu^{2+} species.[24] The spectra of the samples activated under vacuum and treated with O_2 contain at least two poorly resolved signals with $g_{||} = 2.27$–2.32 and $g_{\perp}$ at around 2.04, which is in agreement with previously reported data for Cu-containing ZSM-5.[6m,24a,25] Such parameters are indicative of Cu^{2+} sites with C_{4v}, C_{3v}, and D_{4h} oxygen environments.[24a,26]

Double integration of the EPR spectra shown in Figure 3 was used to measure the concentration of EPR-active Cu^{2+} species (spins) in Cu^{2+}/H-ZSM-5. The obtained data are shown in Table 2 and are discussed below.

The State of Copper Sites in the Zeolite Sample

The data obtained by EXAFS and UV-vis DRS are complementary and allow us to make the following conclusions. The main state of copper in the Cu^{2+}/H-ZSM-5 samples, activated and treated with O_2, is Cu^{2+} cations coordinated by four O-ligands. These O-ligands are from the zeolite ZSM-5 framework (Si–O^-–Al and Si–O–Si sites) as illustrated in previous theoretical and experimental work on EPR characterization of Cu^{2+}

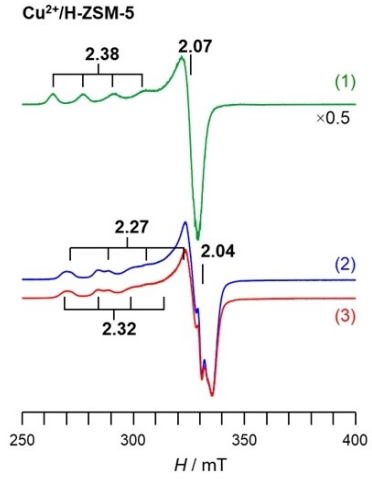

Figure 3. EPR spectra of Cu^{2+}/H-ZSM-5 samples: as-synthesized (green line, 1), after vacuum activation at 673 K (blue line, 2), and further treated with O_2 at 673 K (red line, 3).

Table 2. Cu^{2+} spin concentration[a] (μmol g^{-1}) in Cu^{2+}/H-ZSM-5 zeolite samples under different conditions.

Sample	Before CH4 adsorption	CH4 adsorbed (298 K)	CH4 adsorbed (523 K)
as-synthesized	220	–	–
activated	130	80	25
O_2-treated	120	100	20

[a] The accuracy of the EPR quantitative method is about 30%.

cationic sites in ZSM-5 zeolite.[24a] The presence of the copper-oxo clusters was also detected for Cu^{2+}/H-ZSM-5 by UV-vis DRS (Figure 2), however, their number is minor because no signs of these species were detected by EXAFS (Figure 1c). Therefore, a possible effect of copper-oxo clusters on methane activation will not be considered further.

The effect of vacuum activation of Cu^{2+}/H-ZSM-5 zeolite at 673 K (apart from water removal) is the reduction of some Cu^{2+} sites to Cu^{+} state,[27] which is a reversible process according to EXAFS and UV-vis DRS data (Figures 1c and 2). The zeolite sample treatment with O_2 at 673 K leads to Cu^{+} transformation to Cu^{2+} and an increase in the number of O-ligands in Cu ion coordination sphere, which may result in copper-oxo clusters (e.g., $[Cu_3(\mu\text{-}O)_3]^{2+}$) formation. However, as we have noted above their quantity is low. Thus, it is reasonable to suggest that the reduction process involves such copper-oxo clusters and leads to the formation of the reduced and O-ligand deficient copper-oxo clusters, for instance, $[Cu_3(\mu\text{-}O)_2]^{2+}$ species as reported previously.[6e]

The data on BAS concentration (framework Si–O(H)–Al groups) obtained by ^{1}H MAS NMR method for the parent H-ZSM-5 and Cu^{2+}/H-ZSM-5 samples (Tables 3 and 4) show that there is a remarkable difference in this parameter between the H-form and Cu-modified zeolite. Importantly, BAS concentration remains unchanged for the samples activated under vacuum and treated with O_2. Having determined the BAS concentration and the Cu/Al atomic ratio, the unit cell composition and copper species concentration were assessed for the Cu^{2+}/H-ZSM-5 sample (Table 3) considering the presence of both Cu^{2+} cations and oxo-clusters, $[Cu_3(\mu\text{-}O)_2]^{2+}$ or $[Cu_3(\mu\text{-}O)_3]^{2+}$, in the sample. The results confirm that Cu^{2+} cations are the major state of copper in Cu^{2+}/H-ZSM-5 samples. Indeed, the obtained concentration of Cu^{2+} cations (210 μmol g^{-1}) is in line with the total content of Cu in the sample of 1.38 wt% which gives the estimated number of Cu atoms of 215 μmol g^{-1}. Hence, the ^{1}H MAS NMR results support the observations made by both EXAFS and UV-vis DRS regarding the state and composition of copper species in Cu^{2+}/H-ZSM-5.

It is interesting to compare Cu^{2+} concentrations obtained directly by EPR (Table 2) and assessed based on ICP-OES and ^{1}H MAS NMR data on the total copper content and BAS concentration (Tables 3 and 4). In the case of the sample treated with O_2, which contains copper predominantly in the Cu^{2+} state, the number of EPR-visible spins (120 μmol g^{-1}) amounts to only half of that resulting from the total copper content (215 μmol g^{-1}) or as detected by EPR for the as-synthesized sample (220 μmol g^{-1}). The same trend of EPR-silent Cu^{2+} species in Cu-containing zeolites after water removal was reported earlier.[22,24a,28] This phenomenon was accounted for by several reasons: (i) the formation of antiferromagnetic Cu^{2+} pairs ($S=0$), for instance, in Cu^{2+}–O^{2-}–Cu^{2+} structures;[18a] (ii) the coordination of extra-framework O-ligand (O^-, OH^-) to isolated Cu^{2+} sites;[24a,28e] (iii) the change in isolated Cu^{2+} cation coordination (symmetry decrease) and, as the result, fast relaxation;[28c,d] (iv) weak magnetic interaction of Cu^{2+} cations located in close proximity (4–7 Å).[22,28a,d] Importantly, possible reduction of Cu^{2+} to Cu^{+} state was experimentally excluded from the list[22,28c,d] as additionally supported by the data reported in this work. The intact BAS concentration after the sample treatment with O_2, as compared to the vacuum-activated Cu^{2+}/H-ZSM-5, implies that Cu^{2+} sites do resist reduction during vacuum activation at 673 K (at least for the current Cu/Al ratio). It is also obtained that the number of Cu–O–Cu sites is low (present as $[Cu_3(\mu\text{-}O)_3]^{2+}$) in the studied samples as expected for Cu/Al $\leq$0.3.[16,28c] Additionally, the presence of extra-framework O-ligands for Cu^{2+} cations is not confirmed by UV-Vis DRS. Thus, only two options are left, namely, isolated Cu^{2+} cations with low coordination symmetry and weak-magnetically interacting Cu^{2+} cations (further referred to as paired sites). For the latter species, the interaction Cu–Cu distance is suggested to be longer than can be reliably detected by EXAFS,[22] therefore, such paired Cu^{2+} cations are considered to be isolated in terms of EXAFS but weakly interacting in terms of EPR and magnetic susceptibility study.[28d]

For Cu^{2+}/H-ZSM-5, it is, therefore, reasonable to suggest that Cu^{2+} cations are mostly present as isolated (>7 Å) and paired Cu^{2+} cations (4–7 Å) with no extra-framework O-ligands. The exact proportion between these two types of copper species is difficult to determine precisely. However, taking into account the quantitative EPR data, it can be accepted that a maximal quantity of paired sites does not exceed half of the total number of Cu^{2+} cations.

Table 3. Zeolite unit cell composition[a] and Cu^{2+} and $[Cu_3(\mu\text{-}O)_n]^{2+}$ species concentration[b] (μmol g^{-1}) in Cu^{2+}/H-ZSM-5 zeolite.

Sample	Unit cell composition	Cu^{2+}	$[Cu_3(\mu\text{-}O)_n]^{2+}$
H-ZSM-5	$\lvert H_{5.4}\rvert[Al_{5.4}Si_{90.6}O_{192}]$	–	–
Cu^{2+}/H-ZSM-5	$\lvert Cu^{2+}{}_{1.2}[Cu_3(\mu\text{-}O)_n]^{2+}{}_{0.1}H_{2.8}\rvert$ $[Al_{5.4}Si_{90.6}O_{192}]^{[c]}$	210	20

[a] Estimated based on Cu/Al ratio and BAS concentration (Table 4). [b] Estimated based on unit cell composition. [c] Parameter n equals 2 for the activated sample and 3 for O_2-treated one.

Table 4. Properties of zeolite samples.

Sample	Si/Al[a]	Cu[b]/wt %	Cu/Al[c]	BAS concentration[c]/ μmol g^{-1}
H-ZSM-5	17	–	–	940
Cu^{2+}/H-ZSM-5	17	1.38	0.29	485

[a] Obtained from ^{29}Si MAS NMR. [b] ICP-OES data on Cu and Al contents (wt%). [c] Measured by ^{1}H MAS NMR method, the accuracy is 5–10%.

Methane Activation by Cu^{2+} Cations in ZSM-5 Zeolite

Copper Site Evolution at Methane Adsorption and Activation: UV-Vis DRS and EPR Data

The UV-vis DR spectra for Cu^{2+}/H-ZSM-5 samples with adsorbed methane are presented in Figure 4. After methane adsorption at room temperature (296 K) on the activated sample (Figure 4a), the intensity of the bands at 44200 and 13900 cm^{-1} remarkably increases, and the band at 32000 cm^{-1} appears. It can be suggested that the latter band originates from methane adsorption on O-ligand deficient copper-oxo clusters (for example, $[Cu_3(\mu\text{-}O)_2]^{2+}$). If methane was adsorbed on the O_2-treated Cu^{2+}/H-ZSM-5 sample (Figure 4b), no changes were observed in the spectrum. In this case, O-atoms restore defects in the copper-oxo clusters forming $[Cu_3(\mu\text{-}O)_3]^{2+}$ species and occupying the sites for methane adsorption. The heating of the samples at 523 K with adsorbed methane leads to a drastic decrease in the intensity of all the bands (Figure 4). This demonstrates Cu^{2+} to Cu^{+} reduction caused by methane chemical transformation.

EPR spectra of Cu^{2+}/H-ZSM-5 samples with adsorbed methane are presented in Figure 5. The parameters of the signals (Figure 5, lines 1 and 3) remain the same as for the zeolites before CH_4 adsorption (Figure 3, lines 2 and 3) apart from a slight broadening of the spectral lines. Heating of the samples at 523 K results in a significant decrease in the intensity of the observed signals. Spin concentration becomes lower by 3–5 times indicating that EPR active Cu^{2+} sites interact with methane which is in line with the UV-vis DRS data (Figure 4).

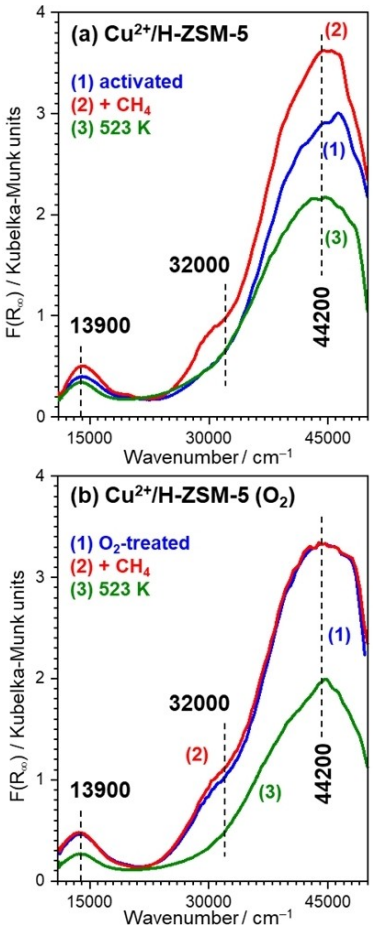

Figure 4. UV-vis DR spectra of the activated (a) and O_2-treated (b) Cu^{2+}/H-ZSM-5 samples: pure zeolite (blue lines, 1), after methane adsorption at 296 K (red lines, 2) and further heating at 523 K for 1 h (green lines, 3).

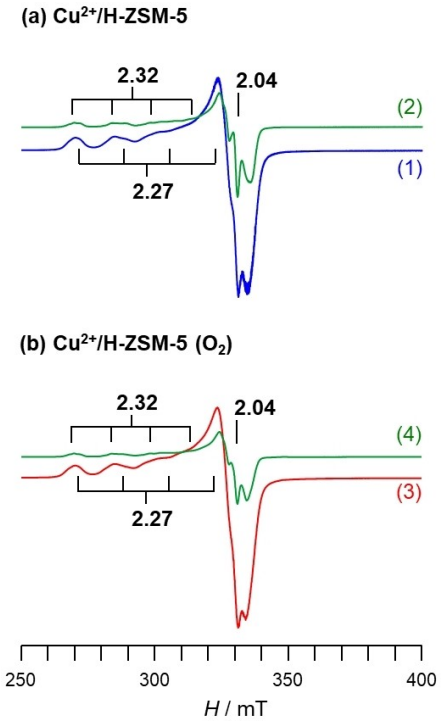

Figure 5. EPR spectra of the activated Cu^{2+}/H-ZSM-5 sample (a) after methane adsorption at 296 K (blue line, 1) and after further heating at 523 K for 1 h (green line, 2). EPR spectra of the O_2-treated Cu^{2+}/H-ZSM-5 sample (b) after methane adsorption at 296 K (red line, 3) and after further heating at 523 K for 1 h (green line, 4).

Thus, the UV-vis DRS and EPR data show the following. Methane strongly interacts with Cu species of Cu^{2+}/H-ZSM-5 sample at room temperature (296 K). This is seen by the absorbance increase in the UV-vis DR spectra at the particular wavenumbers and the broadening of the EPR signals. The evolution of UV-vis DR and EPR spectra indicates the symmetry change of the ligands in the first coordination sphere of the Cu^{2+} sites. Such perturbation can result from methane entrance into the coordination sphere of the Cu^{2+} sites and its relatively strong adsorption on them. Previously, we have observed the formation of methane adsorption complexes on Cu^{2+} cations and $[Cu_3(\mu\text{-}O)_3]^{2+}$ oxo-clusters with the ^{1}H HYSCORE[6m] and FTIR spectroscopy[6m,n] methods. Here, UV-DRS and EPR experiments confirm our earlier finding. In such a complex, methane experiences strong polarization of the C–H bond which makes its further chemical transformation possible.

It should be noted that methane transformation (at 523 K) on the Cu^{2+}/H-ZSM-5 samples leads to the reduction of Cu^{2+} sites existing in the form of isolated or paired Cu^{2+} cations. Therefore, the presented data evidence that these two types of

copper species may be involved in the activation and further chemical transformation of methane.

Evidence for Methane Transformation by ^{13}C MAS NMR Spectroscopy

Figure 6 shows ^{13}C CP/MAS NMR spectra of the surface species formed after methane transformation on the zeolite samples at 523 K. Full-range ^{13}C MAS NMR and ^{13}C CP/MAS NMR spectra are found in Figures S4 and S5. Methane transformation on Cu^{2+}/H-ZSM-5 starts at 473 K and the methoxy-like species are detected on the zeolite surface up to 573 K. Note that the parent H-ZSM-5 zeolite is inactive for methane activation and transformation as demonstrated in our previous study.[6m]

Depending on the conditions, two or three signals in the specific region of 53–63 ppm are detected (Figure 6). In our recent works,[6l,29] the assignment of the detected signals to particular methoxy species has been suggested based on ^{13}C MAS NMR and DFT data. The resonance at 63 ppm belongs to the methoxy-like Cu–O(CH_3)–Cu or Cu(CH_3OH)Cu species formed after methane interaction with the reactive Cu–O–Cu sites of bi- and trinuclear copper-oxo clusters, for instance, $[Cu_2(\mu\text{-}O)]^{2+}$ or $[Cu_3(\mu\text{-}O)_3]^{2+}$. The absence of this signal in the spectrum of methane on activated Cu^{2+}/H-ZSM-5 (Figure 6a) and its appearance in the spectrum for O_2-treated Cu^{2+}/H-ZSM-5 (Figure 6b) confirm such an assignment because the presence of a small quantity of $[Cu_3(\mu\text{-}O)_3]^{2+}$ oxo-clusters was observed by UV-vis DRS (Figure 2). The signal at 58 ppm arises from the methyl groups attached to the zeolite framework, i.e. by Si–O(CH_3)–Al fragments. The third signal at 53 ppm originates from methanol adsorbed on zeolite BAS.

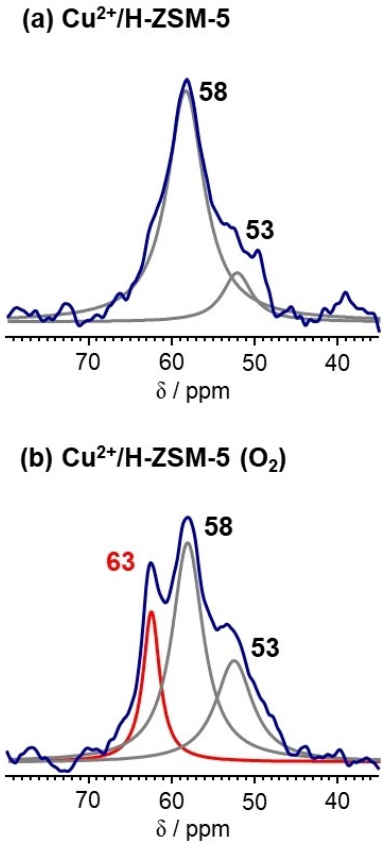

Figure 6. ^{13}C CP/MAS NMR spectra of the methoxy-like species formed after methane-^{13}C reaction at 523 K for 1 h on the vacuum activated (a) and O_2-treated (b) Cu^{2+}/H-ZSM-5. Full-range ^{13}C (CP) MAS NMR spectra are shown in Figures S2 and S3. The model spectra obtained after fitting are shown in Figure S6.

The highest concentration of the methoxy-like species is observed at 523 K (Figure S4). The relative integrated intensity of the signals at 53–63 ppm is 8% and 5% for the activated and O_2-treated Cu^{2+}/H-ZSM-5 samples, respectively. For the former case, this amounts to 24 μmol of methoxy-like species per zeolite gram (initial concentration of methane-^{13}C is 300 μmol g^{-1}). Such value is equivalent to 0.11 mol of extracted methanol per 1 mol of Cu^{2+} cations in the zeolite (or 0.09 mol CH_3OH per 1 mol Cu-total).

Importantly, the ^{13}C MAS NMR data for the activated Cu^{2+}/H-ZSM-5 sample support our conclusion on the properties of Cu^{2+} cations to provide activation and further chemical transformation of methane. According to the results obtained in this work, this type of copper sites transforms methane into surface methoxy-like species and methanol. Therefore, it is important to inquire into the mechanisms of methane activation and its transformation to methanol on Cu^{2+} cationic species in ZSM-5 zeolite.

Methane Activation on Isolated Cu^{2+} Cations

The activated Cu^{2+}/H-ZSM-5 sample demonstrates the formation of the two surface methoxy-like species as a result of methane activation and transformation, namely, Si–O(CH_3)–Al species and methanol adsorbed on BAS (Figure 6a). In our earlier work,[6m] we have presumed that methane C–H bond dissociation on isolated Cu^{2+} cations occurs through the heterolytic pathway with the formation of surface Si–O(CH_3)–Al and copper hydride species ("carbenium" pathway). Alternatively, the "alkyl" pathway of heterolytic C–H bond dissociation could be considered,[30] which may result in BAS (Si–O(H)–Al) and methylcopper species. In this regard, we have performed the DFT calculations to compare these two pathways and establish the mechanisms of methane C–H bond activation with the assistance of isolated Cu^{2+} cations.

Our calculations (Figure 7) show that the previously suggested "carbenium" pathway is strictly unfavorable with an intrinsic activation barrier of 320 kJ mol^{-1}. On the other hand, the "alkyl" pathway is characterized by the activation energy of 95 kJ mol^{-1}. Therefore, the DFT method shows that methane activation on isolated Cu^{2+} cations should occur with the formation of the Cu-methyl species similar to alkane C–H bond dissociation on the Zn, Ga, and In-containing zeolites.[4c,31]

^{13}C MAS NMR does not detect any surface species apart from methoxy-like ones (Figures S4 and S5). This can be due to the broadening or shift of the ^{13}C NMR signal of the methyl group bonded directly to the paramagnetic Cu^{2+} site. Usually,

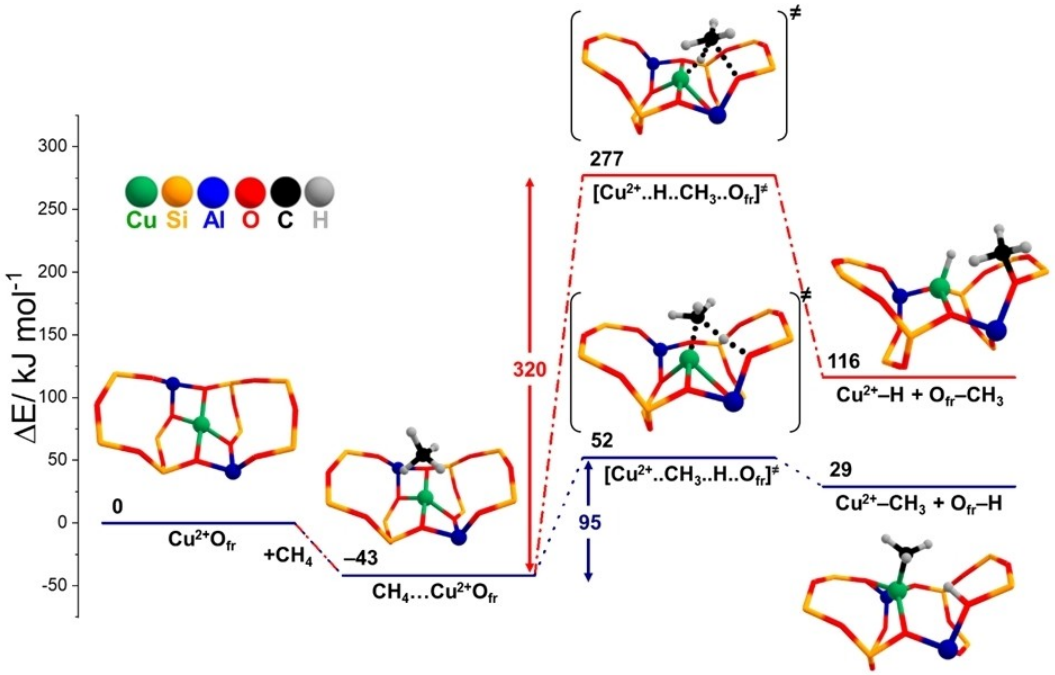

Figure 7. Possible pathways of methane C–H bond dissociation on isolated Cu^{2+} cations in Cu^{2+}/H-ZSM-5 zeolite. O_{fr} denotes one of the Si–O^-–Al sites of ZSM-5 zeolite to which a Cu^{2+} cation is attached.

the methyl group attached to a metal atom exhibits the chemical shift at −40–0 ppm.[32]

To clarify this, we have applied FTIR spectroscopy to monitor the surface species formed from methane on the activated Cu^{2+}/H-ZSM-5 sample (Figure S7). Similar to the ^{13}C MAS NMR result, the formation of only methoxy-like species was observed (see the description for Figure S7). Taking ^{13}C MAS NMR, FTIR, and DFT results into account, it can be suggested that methane activation by Cu^{2+} cations should occur following an alternative pathway.

Methane Activation on Paired Cu^{2+} Sites

To inquire into the mechanism of methane activation by Cu^{2+} cations, we have further analyzed the pathway of methane transformation with the assistance of paired Cu^{2+} sites. Such a state is enabled by the close proximity of copper atoms (~6.1 Å in the considered model, Figure 8) in the zeolite. Initially, we have assumed that methane activation on paired Cu^{2+} cations could be performed similarly to methane activation on bi- and trinuclear copper-oxo clusters,[6e] i.e. by homolytic C–H bond cleavage, which is driven by a high spin density on the extra-framework oxygen atoms of copper-oxo clusters. However, the calculated Loewdin spin densities for the paired sites are mostly localized on the copper cations, while the spin density on the framework oxygen atoms is negligible (Figure S8). Therefore, the homolytic pathway is not possible. Taking this into account, we suggest an alternative mechanism for methane activation (Figure 8) on Cu^{2+} pairs.

The activation is initiated by methane adsorption on a paired Cu^{2+} site (−48 kJ mol^{-1}) followed by the heterolytic C–H bond dissociation on one of the Cu^{2+} cations (Figure 8). The dissociation results in the formation of the methylcopper species and BAS. This step has an activation energy of 149 kJ mol^{-1} (TS1) which is higher than that for methane C–H bond dissociation on an isolated Cu^{2+} site (95 kJ mol^{-1}, Figure 7) due to less constrained local confinement of isolated Cu^{2+} cation. Further, the formed Cu–C bond splitting occurs (TS2) simultaneously with the electron transfer from the carbon atom to a copper one, resulting in the methyl group migration on the second Cu^{2+} site and the reduction of the first one to Cu^+ state. This step has a low activation barrier of 42 kJ mol^{-1}. The methyl radical is stabilized on the second copper cation that retains an oxidation state of +2. However, such a structure has relatively high energy, therefore, the methyl radical rebounds to the framework Si–O^-–Al site with the electron transfer to the Cu^{2+} site. The products of this step, proceeding without an activation barrier, are Si–O(CH_3)–Al species and Cu^+ cation. As follows from the described reaction pathway (Figure 8), methane transformation on a paired Cu^{2+} site results in Si–O(CH_3)–Al and Si–O(H)–Al species as well as in the reduction of both copper sites to Cu^+ state. Regarding the observed methoxy-like species (Figure 6a), it can be now concluded that these species are formed as the result of methane activation by paired Cu^{2+} sites. The performed calculations show that methane can be transformed into the surface methoxy species by the paired Cu^{2+} sites with no extra-framework O-ligand required.

To validate the described mechanism, the reported UV-vis DRS data in Figure 4a can be used. Comparing the spectra presented by lines 1 and 3 (line 2 is ignored since the spectrum

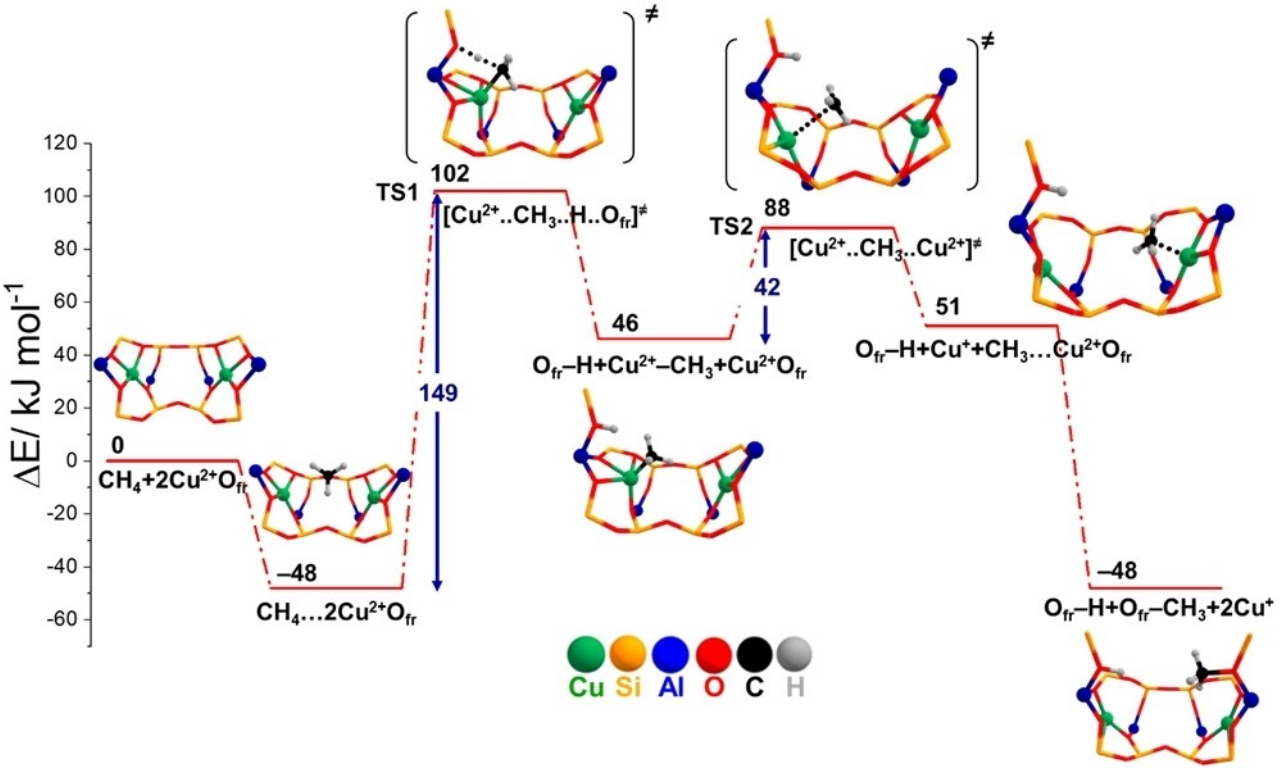

Figure 8. Possible pathway of methane C–H bond dissociation on a paired Cu^{2+} site resulting in methoxy species formation in Cu^{2+}/H-ZSM-5 zeolite. O_{fr} denotes one of the Si–O^-–Al sites of ZSM-5 zeolite to which a Cu^{2+} cation is attached.

is perturbed by methane adsorption on the active Cu^{2+} sites), it can be seen that the intensity of the band at 44200 cm^{-1} (exhibited by Cu^{2+} cations) decreases by about 1.4 times as the result of Cu^{2+} site reduction to Cu^{+} upon methane activation and transformation. This means that 29% of Cu^{2+} sites (60 μmol g^{-1}) participate in the reaction with methane. According to the mechanism presented in Figure 8, methane reaction with paired Cu^{2+} sites should result in one methoxy group per two Cu^{2+} cations consumed. Therefore, one can expect the formation of 30 μmol g^{-1} of methoxy-like species which is close to the number of the species (24 μmol g^{-1}) detected by ^{13}C MAS NMR (*vide supra*). Thus, the suggested mechanism agrees well with the quantitative data provided by UV-vis DRS and ^{13}C MAS NMR methods.

Additional confirmation for the suggested mechanism can be found in ^{1}H MAS NMR spectra shown in Figure 9. The spectra demonstrate that BAS concentration increases after methane activation on the activated Cu^{2+}/H-ZSM-5 zeolite (Figure 9a and b), which is predicted by our DFT calculations as shown in Figure 8. ^{1}H MAS NMR detects bridged Si–O(H)–Al groups (BAS) at 3.9 and 5–6 ppm (isolated and H-bonded, respectively) and terminal Si–OH groups at 1.8 ppm.[33]

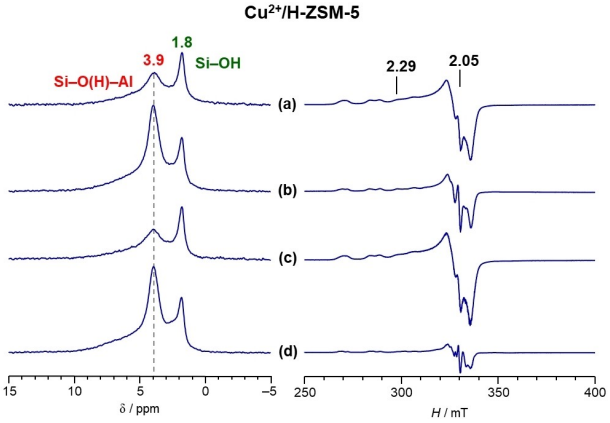

Figure 9. ^{1}H MAS NMR and EPR spectra of Cu^{2+}/H-ZSM-5: activated under vacuum at 673 K (a), after methane reaction at 523 K for 1 h (b), O_2-regenerated at 773 K for 0.5 h (c), H_2O-treated at 473 K for 1 h (d). Unreacted methane, O_2, and H_2O were removed from the zeolite samples (see Experimental section).

Methanol Formation and Paired Cu^{2+} Site Regeneration

We have calculated the energy profile (Figure 10) demonstrating a further possible pathway of the surface Si–O(CH_3)–Al species removal. This can be achieved by water addition which converts the methoxy species to a methanol molecule and a new BAS through a step with the activation barrier of 117 kJ mol^{-1} (TS3). This step occurs through the intermediate stabilization of protonated methanol molecule $[CH_3OH_2]^+$ which, however, has relatively high energy and, therefore, transforms further to methanol and BAS (deprotonation) without the activation barrier. The formed methanol molecule is strongly bound to a BAS but can be desorbed from the zeolite

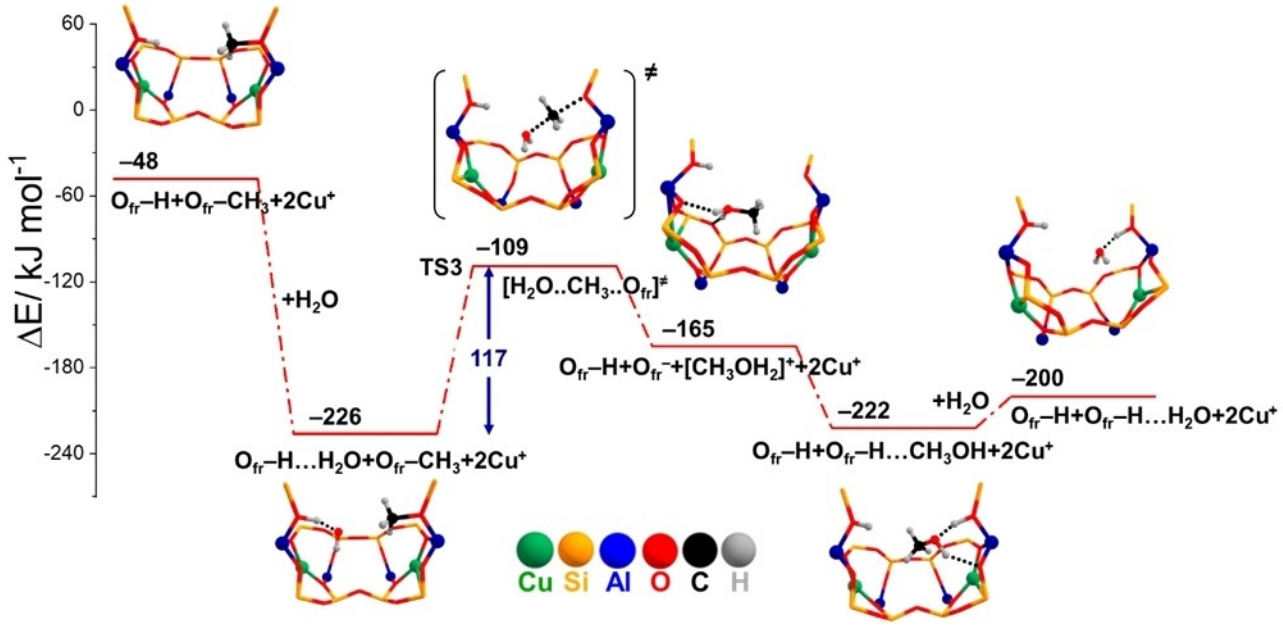

Figure 10. Possible pathway of methoxy species, formed from methane with the assistance of a paired Cu^{2+} site, transformation to methanol on Cu^{2+}/H-ZSM-5 zeolite. O_{fr} denotes one of the Si–O^-–Al sites of ZSM-5 zeolite to which a Cu^{2+} cation is attached.

by adding another water molecule (the last step in Figure 10), which has been demonstrated experimentally.[34] After methane activation and methanol desorption, the resulting state of the considered model, representing Cu^{2+}/H-ZSM-5 zeolite, is reduced paired Cu^+ site, two BAS, and a water molecule adsorbed.

The formed Cu^+ sites are not active for methane activation and transformation as follows from a recent report[35] and the data shown in Figure S9. The regeneration of the copper species in zeolites can be performed by oxidation with molecular oxygen[36] or water,[6g] though the latter option is debatable.[37] Here, we studied two possible ways to regenerate the initial Cu^{2+} paired sites with O_2 or H_2O by ^{1}H MAS NMR and EPR methods, which were used to monitor zeolite BAS and Cu^{2+} sites, respectively. Figure 9 shows the obtained results. After methane reaction on the activated Cu^{2+}/H-ZSM-5 zeolite, BAS concentration increases and the number of Cu^{2+} cations decreases simultaneously due to the reduction to Cu^+ (compare Figures 9a and b). This is seen by the increased intensity of the signal at 3.9 ppm and decreased intensity of the EPR resonances, which become better resolved due to fewer Cu^{2+} spins. Further, the spent zeolite was treated with either O_2 at 773 K or H_2O at 473 K in an attempt to regenerate copper sites. Figures 9a and c demonstrate that the zeolite returns to its initial state in terms of BAS and Cu^{2+} concentration after the treatment with O_2. On the contrary, for the zeolite treated with H_2O, the number of BAS remains almost the same as it was observed after the reaction with methane, whereas the concentration of Cu^{2+} cations slightly decreases (compare Figures 9b and d). This implies that Cu^{2+} cations in ZSM-5 zeolite can be regenerated only by the treatment with O_2 but not with H_2O, at least under the conditions of our experiments.

Conclusions

In this study, the mechanism of methane activation on Cu-modified H-ZSM-5 zeolite (Cu^{2+}/H-ZSM-5), loaded with Cu^{2+} cations, was studied. The zeolite sample was investigated by UV-vis DRS, EPR, EXAFS, FTIR spectroscopy, and MAS NMR methods with respect to the state and evolution of the copper sites and the surface species formed during methane activation and transformation. The DFT method was applied to analyze the possible pathways of methane C–H bond dissociation with the assistance of copper cationic sites in ZSM-5 zeolite.

The state of the copper species was characterized by UV-vis DRS, EPR, and EXAFS methods during the vacuum activation and subsequent treatment with O_2 of the zeolite samples as well as upon interaction with methane. Our results demonstrate that, in Cu^{2+}/H-ZSM-5, copper is mostly present in the form of Cu^{2+} cations, isolated and paired ones.

^{13}C CP/MAS NMR and FTIR spectroscopy detected the formation of different methoxy-like species from methane activated on Cu^{2+}/H-ZSM-5. To understand possible pathways of methane activation on Cu^{2+} cations, DFT calculations were performed. Although DFT results show that the heterolytic dissociation, resulting in Cu–CH_3 species and BAS, is a preferable pathway for methane C–H bond activation on Cu^{2+} cations, it occurs only for paired sites. Further transformation of the Cu–CH_3 species on paired Cu^{2+} sites could follow the pathway: (i) methyl radical formation after breaking Cu–C bond and (ii) the radical recombination with the zeolite Si–O^-–Al site. This reaction results in additional BAS, surface Si–O(CH_3)–Al species, and two Cu^+ cations, as observed by MAS NMR, FTIR, UV-vis DRS, and EPR methods.

It was experimentally obtained that Cu^{2+} cations in ZSM-5 zeolite could be regenerated only by the treatment with O_2 but not with H_2O.

Experimental

Reagents and Materials

Copper(II) acetate monohydrate (≥98%), methane-^{13}C (99% ^{13}C), were purchased from Aldrich Chemical Co. Inc. CH_4 (99.9%) and O_2 (99.9%) were industrially produced gases. Methane-^{13}C, methane, and molecular oxygen were used after water trace removal at liquid nitrogen temperature via freezing and thawing circles.

Zeolite Sample Preparation and Characterization

An H-form of ZSM-5 zeolite (H-ZSM-5) provided by Novosibirsk Chemical Concentrates Plant, Novosibirsk, Russia was used for copper species loading. ^{27}Al and ^{29}Si MAS NMR analysis revealed a Si/Al ratio of 17 and 4% extra-framework aluminum species (Figure S10). The content of 2.05 wt% for aluminum and 0.09 wt% and 0.05 wt% for iron and sodium impurities, respectively, was obtained by elemental analysis (ICP-OES).

Zeolite containing Cu^{2+} cations (denoted further as Cu^{2+}/H-ZSM-5) was prepared by the ion exchange of H-ZSM-5 with copper acetate solution.[21] Copper concentration in the solution was 0.039 M.[38] Weight concentration of the zeolite in water suspension was 10 wt%. After the ion exchange, Cu^{2+}/H-ZSM-5 was dried at 393 K and further calcined in airflow and 773 K. The sample is referred to as as-synthesized". Such sample was kept under ambient atmosphere before spectroscopic measurements.

The amount of copper loaded in the Cu^{2+}/H-ZSM-5 sample was 1.38 wt% (Cu/Al = 0.29) as obtained by the ICP-OES method. The state of the copper species was analyzed by UV-vis DRS, EPR, and EXAFS (*vide supra*). The sample was also characterized by ^{1}H MAS NMR method to measure the quantity of Brønsted acid sites (BAS, bridged Si–O(H)–Al groups).[33a] Table 4 shows some characteristics for the Cu^{2+}/H-ZSM-5 sample.

Sample Preparation for Spectroscopic Studies

For spectroscopic experiments, zeolite samples were treated according to the following activation procedure: (i) evacuation at 673 K for 18 h under vacuum with a residual pressure above the sample of $<10^{-3}$ Pa; (ii) treatment with pure O_2 (industrially produced gas, 99.9%), if needed, under the static pressure of 500 mbar for 1 h at 673 K followed by evacuation at 423 K for 1 h. The sample evacuated at 673 K is referred to as „activated" while the sample which was additionally treated with O_2 is referred to as „O_2-treated". These samples were kept sealed inside the spectroscopic cell or NMR ampules before and during spectroscopic measurements.

For UV-vis DRS experiment, approximately 200 mg of zeolite powder were activated inside special homemade glassware (Figure S11) that was directly connected to a UV-vis cell. This cell is made of optical-grade and UV-transparent quartz glass and equipped with a valve through which methane can be dosed inside the cell. Methane (industrially produced gas, 99.9%) was dosed inside the cell up to the pressure of 100 mbar to study the interaction of methane with copper sites *in situ*.

For EXAFS measurement, approximately 900 mg of zeolite powder was activated inside a glass ampule. After the activation procedure, the ampule was sealed off with a micro-torch flame to preserve the sample. Before the measurement, the ampule was unsealed under Ar atmosphere inside a glovebox, and the zeolite powder was transferred into a homemade EXAFS cell.

For ^{13}C MAS NMR experiment, a zeolite sample (20–30 mg) was put into a high-axially symmetric glass ampule (which is made of a borosilicate glass tube of 3.0 mm outer diameter) and activated with the procedure mentioned above. After activation, the zeolite sample was loaded with methane-^{13}C, with the concentration of adsorbed methane being equal to 300 $\mu mol\,g^{-1}$, at 77 K (liquid nitrogen) followed by sealing the ampule off with micro-torch flame. Such glass ampule (length of about 10 mm) could be tightly inserted in 4 mm zirconia MAS NMR rotors for in situ ^{13}C MAS NMR analysis of the products of methane interaction with copper sites.

EPR measurements were performed using the samples prepared for ^{13}C MAS NMR experiments by putting them into the borosilicate glass tube of 5.0 mm outer diameter and 7-inch length (Wilmad NMR tube).

Zeolite Sample Regeneration

Separate experiments were performed to study possible approaches to regenerate Cu^{2+} sites in Cu^{2+}/H-ZSM-5 zeolite after the reaction with methane. Four samples were prepared and further analyzed by ^{1}H MAS NMR and EPR methods. For each sample, the same amount of zeolite was used (35 mg) which was placed in a special glass cell of 3.3–3.9 cm^3 in volume (Figure S12).

To prepare the first sample, Cu^{2+}/H-ZSM-5 zeolite was activated at 673 K for 18 h under vacuum, and a glass cell was sealed off with micro-torch flame. The activated zeolite was transferred to a MAS NMR ampule which was further sealed off.

For the second sample, Cu^{2+}/H-ZSM-5 zeolite was activated at 673 K and further exposed to methane pressure. To do that, the methane was first dosed into a calibrated volume of the vacuum line at room temperature (296 K) and then transferred into the cell containing zeolite by freezing with liquid nitrogen. The cell was sealed off under the residual methane pressure of 14 mbar. The amount of methane dosed into the calibrated volume was selected to create a pressure of about 2 bar inside the cell at room temperature. The sealed cell with the activated zeolite and methane inside was heated at 523 K for 1 h. Afterward, an excess of unreacted methane was evacuated from the cell at room temperature up to a pressure of $<10^{-3}$ Pa. The cell was again sealed off, zeolite was transferred into an ampule which was sealed off.

To prepare the third sample, Cu^{2+}/H-ZSM-5 zeolite was activated at 673 K and reacted with methane at 523 K (following the procedure described above). Then, methane was removed from the cell and the zeolite was exposed to a static pressure of O_2 (600 mbar) at 773 K for 0.5 h (the cell was connected to the vacuum line). Afterward, the O_2-regenerated zeolite was again evacuated under vacuum at 673 K for 18 h, with the cell and NMR ampule being subsequently sealed off.

The fourth sample was prepared as follows. Cu^{2+}/H-ZSM-5 zeolite was activated at 673 K and reacted with methane at 523 K, with methane being further evacuated. Then, the zeolite was exposed to H_2O pressure of 25 mbar at 296 K. H_2O vapor was transferred into the cell containing zeolite at 77 K. The cell was sealed off and heated at 473 K for 1 h. The water was removed from the H_2O-treated zeolite under vacuum at 473 K for 3 h followed by

evacuation at 673 K for 18 h. The NMR ampule with the zeolite inside was sealed off.

All four samples were studied with ^{1}H MAS NMR and EPR methods. For the study with EPR, MAS NMR ampule with the zeolite sample was inserted into the borosilicate glass tube of 5.0 mm outer diameter and 7-inch length (Wilmad NMR tube).

Ultraviolet-Visible Near-Infrared Diffuse Reflectance (UV-vis DR) Spectroscopy

A Shimadzu UV-2501 PC spectrophotometer equipped with an ISR-240 diffuse reflectance accessory was used to record the UV-vis DR spectra. The spectral range of 11000–53000 cm^{-1} was monitored with respect to the $BaSO_4$ reflectance standard. The obtained spectra are presented in the Kubelka-Munk units: $F(R_\infty)$ vs wave-number.

Electron Paramagnetic Resonance Spectroscopy

Pulse EPR measurements were carried out at a temperature of liquid nitrogen (about 77 K) using a CMS 8400 spectrometer. The following parameters were used for EPR spectra acquisition: working frequency of 9.4 GHz, modulation amplitude of the magnetic field of 0.5 mT, modulation frequency of 100 kHz, and magnetic field sweep rate of 1 mT/s. The values of the g-factors for the signals were determined using an external standard, 10^{-3} M TEMPO solution in toluene ($g = 2.00$). For quantitative assessment of Cu^{2+} spin concentration, a monocrystal of $CuCl_2{\times}2H_2O$ was used as an external standard with a spin number of $3.3{\times}10^{17}$. The relative accuracy of the approach is about 30%.

Solid State Magic Angle Spinning Nuclear Magnetic Resonance Spectroscopy (SS MAS NMR)

NMR spectra were recorded using a Bruker Avance-400 spectrometer (9.4 T) equipped with a broad-band double-resonance MAS probe. The chemical shift was referenced[39] to TMS for ^{1}H, ^{13}C, and ^{29}Si NMR spectra and 0.1 M $Al(NO_3)_3$ solution for ^{27}Al NMR with an accuracy of ± 0.1 ppm.[40]

The glass ampules with the samples of activated zeolite were inserted into the zirconia rotor that was spun at 5 kHz by compressed air. For ^{1}H MAS NMR spectra Hahn-echo pulse sequence $\pi/2-\tau-\pi-\tau$ acquisition, where τ is equal to one rotor period, was used. $\pi/2$ pulse of 6.0 μs was used for proton excitation. 32 scans with a 60 s delay were accumulated. ^{13}C MAS NMR spectra were obtained with high-power decoupling, and 2000 scans with 5 s delay were recorded. For ^{13}C CP/MAS NMR spectra, the proton high power decoupling field strength was 11.7 G (5.0 μs length of 90° ^{1}H pulse); contact time was 2 ms at the Hartmann – Hahn matching condition of 50 kHz; the delay between scans was 2 s. 40000 scans were acquired.

^{27}Al and ^{29}Si NMR spectra were recorded with the use of 4 mm rotors filled with zeolite powder preliminary kept under a moist atmosphere for several hours. A spinning rate of 10–15 kHz was used. ^{27}Al MAS NMR spectra were obtained with a short 0.6 μs pulse ($\pi/12$), and 10 000 scans were accumulated with a 0.5 s recycle delay. ^{29}Si MAS NMR spectra were recorded with a 5.0 μs pulse ($\pi/2$) and 60 s repetition time, and 1000 scans were acquired for signal accumulation.

Density Functional Theory Calculations

ZSM-5 zeolite unit cell of the MFI framework type was represented by the molecular clusters containing 40 T-atoms (for isolated Cu^{2+} site) and 34 T-atoms (for paired $Cu^{2+}\ldots Cu^{2+}$ sites) (Figure S13). The initial MFI-type structure was taken from the Database of Zeolite Structures.[17] To compensate for the charge of extra-framework Cu^{2+} cation, aluminum atoms were placed in T7 and T12 positions of the ZSM-5 framework.[6e] For the structures with two Cu^{2+} cations, two pairs of silicon atoms at T5 and T11 positions were replaced with aluminum atoms. The terminal framework oxygen atoms in the clusters were replaced by H atoms at distances of 1.47 Å from Si atoms. These H atoms were fixed during all geometry optimizations to avoid unrealistic distortions of the zeolite framework.[29]

Spin-unrestricted DFT calculations were carried out using the ORCA 5.0.2 program package.[41] Hybrid exchange-correlational PBE0 functional was used to describe the exchange-correlational term.[42] To account for the dispersion interactions, D3BJ correction was applied.[43] 6–31G* basis set[44] was used for the zeolite framework (Si, Al, O) and terminal H atoms ($H_{terminal}$) while def2-TZVP basis set[45] was applied for the extra-framework atoms (Cu, C, H). Transition states were identified using the CI-NEB procedure[46] as implemented in ORCA.[41]

For all calculations by ORCA, the default convergence criteria were used. Specifically, the SCF iteration was considered converged when the energy difference between successive steps was less than $1{\times}10^{-8}$ Hartree. The geometry optimization was considered complete when the energy difference between successive geometries was less than $5{\times}10^{-6}$ Hartree, and the root-mean-square and maximum energy gradients were less than $1{\times}10^{-4}$ Hartree/Bohr and $3{\times}10^{-4}$ Hartree/Bohr, respectively.

Extended X-Ray Absorption Fine Structure (EXAFS)

The EXAFS (Cu–K edge) spectra for all studied samples were recorded at EXAFS Station of the VEPP-3/VEPP-4 M complex[47] at the Siberian Synchrotron and Terahertz Radiation Center (SSTRC, Novosibirsk) under transmission and fluorescent modes using electron energy of 2 GeV and an average storage ring current of 100 mA during the measurements. A channel-cut Si(111) monochromator was used. The EXAFS spectra were measured using ionizing chambers and fluorescent detectors with a step size of approximately 1.5 eV.

The $\chi(k)$ oscillations were extracted by the standard procedure.[48] The pre-edge part was extrapolated to the EXAFS oscillation region with Victoreen polynomials. The smooth region of the absorption spectrum was formed by the cubic splines. The inflection point of the absorption edge was used as the initial point E_0 of the EXAFS spectrum. The atomic radial distribution functions (RDF) were derived using the Fourier transform modulus $k^3\chi(k)$ in the wave-number interval of 3.0–12.5 $Å^{-1}$. The structural information, i.e., distances (R) and coordination numbers (CN), was obtained by simulating the spectra with VIPER[48] and EXCURV92[49] codes after preliminary resorting with Fourier filtering to published X-ray diffraction data for the reference bulk compounds[14,15] at fixed Debye – Waller factors. The interatomic distances (R) were determined with a standard accuracy of 0.02–0.03 Å. The accuracy for determining coordination numbers (CN) was 10–15%. Fixed values of Debye factors were 0.007–0.008 $Å^2$. The values of the R-factor were within 2–3%. The amplitude reduction factor (S_0^2) was fixed to 0.9. The values of the E_0 were within −3–0 eV. The obtained values of the R-factor were no more than 3%.

Supporting Information Summary

The authors have cited additional references within the Supporting Information.[50] The Supporting Information includes the following data. Experimental details on reagents and materials, zeolite sample preparation and characterization, parameters used for spectroscopic measurements and DFT calculations. EXAFS structural data of the local Cu arrangement for the reference materials. Cu 2p and Cu LMM core-level XPS spectra of the activated Cu^{2+}/H-ZSM-5 zeolite. Powder XRD pattern, HAADF-STEM and EDX elemental mapping images of as-synthesized Cu^{2+}/H-ZSM-5 zeolite. UV-vis DR spectrum of the parent H-ZSM-5 zeolite. ^{13}C (CP) MAS NMR spectra of methane-^{13}C adsorbed on Cu^{2+}/H-ZSM-5 samples. FTIR spectra of methane adsorbed on the activated Cu^{2+}/H-ZSM-5 zeolite. Löwdin spin population on paired Cu^{2+} site. ^{29}Si MAS NMR and ^{27}Al MAS NMR spectra of the parent H-ZSM-5 zeolite. The schematic picture of the homemade UV-vis DRS cell used. The photos of homemade Pyrex glass cells. The cluster models of ZSM-5 zeolite.

Acknowledgements

This work was supported by the Ministry of Science and Higher Education of the Russian Federation within the governmental assignment for Boreskov Institute of Catalysis (project FWUR-2024-0032). Computational resources for DFT calculations were provided by the Computational Center of Novosibirsk State University. The EXAFS studies were supported by the Ministry of Science and Higher Education of the Russian Federation within the governmental order for Synchrotron Radiation Facility SKIF, Boreskov Institute of Catalysis (FWUR-2024-0040). We thank Dr. Igor E. Soshnikov (Boreskov Institute of Catalysis) for his help with EPR spectrum recording and evaluation. We thank Dr. Igor P. Prosvirin (Boreskov Institute of Catalysis) for his help with XPS spectrum recording and evaluation.

Conflict of Interests

The authors declare no conflict of interest.

Data Availability Statement

The data that support the findings of this study are available from the corresponding author upon reasonable request.

Keywords: Methane · Methanol · C–H bond activation · Cu-modified ZSM-5 zeolite · Spectroscopy and DFT

[1] a) G. A. Olah, *Angew. Chem. Int. Ed.* **2005**, *44*, 2636–2639; b) E. McFarland, *Science* **2012**, *338*, 340–342.
[2] L. Sun, Y. Wang, N. Guan, L. Li, *Energy Technol.* **2020**, *8*, 1900826.
[3] a) R. A. Periana, D. J. Taube, E. R. Evitt, D. G. Löffler, P. R. Wentrcek, G. Voss, T. Masuda, *Science* **1993**, *259*, 340–343; b) R. Palkovits, M. Antonietti, P. Kuhn, A. Thomas, F. Schuth, *Angew. Chem. Int. Ed.* **2009**, *48*, 6909–6912; c) L. Wang, J. Jin, W. Li, C. Li, L. Zhu, Z. Zhou, L. Zhang, X. Zhang, L. Yuan, *Energy Environ. Sci.* **2024**, *17*, 9122–9133; d) S. Sogukkanli, T. Moteki, M. Ogura, *Green Chem.* **2021**, *23*, 2148–2154; e) F. Gu, X. Qin, M. Li, Y. Xu, S. Hong, M. Ouyang, G. Giannakakis, S. Cao, M. Peng, J. Xie, M. Wang, D. Han, D. Xiao, X. Wang, Z. Wang, D. Ma, *Angew. Chem. Int. Ed.* **2022**, *61*, e202201540; f) W. Wang, W. Zhou, Y. Tang, W. Cao, S. R. Docherty, F. Wu, K. Cheng, Q. Zhang, C. Copéret, Y. Wang, *J. Am. Chem. Soc.* **2023**, *145*, 12928–12934.
[4] a) J.-F. Wu, S.-M. Yu, W. D. Wang, Y.-X. Fan, S. Bai, C.-W. Zhang, Q. Gao, J. Huang, W. Wang, *J. Am. Chem. Soc.* **2013**, *135*, 13567–13573; b) K. Narsimhan, V. K. Michaelis, G. Mathies, W. R. Gunther, R. G. Griffin, Y. Román-Leshkov, *J. Am. Chem. Soc.* **2015**, *137*, 1825–1832; c) A. G. Stepanov, S. S. Arzumanov, A. A. Gabrienko, *Chem.: Methods* **2021**, *1*, 224–230; d) T. Moteki, N. Tominaga, M. Ogura, *Appl. Catal. B-Environ.* **2022**, *300*, 120742; e) J. Shan, M. Li, L. F. Allard, S. Lee, M. Flytzani-Stephanopoulos, *Nature* **2017**, *551*, 605–608.
[5] a) X. G. Guo, G. Z. Fang, G. Li, H. Ma, H. J. Fan, L. Yu, C. Ma, X. Wu, D. H. Deng, M. M. Wei, D. L. Tan, R. Si, S. Zhang, J. Q. Li, L. T. Sun, Z. C. Tang, X. L. Pan, X. H. Bao, *Science* **2014**, *344*, 616–619; b) Y. Liu, D. Li, T. Wang, Y. Liu, T. Xu, Y. Zhang, *ACS Catal.* **2016**, *6*, 5366–5370; c) Z. X. Xi, B. J. Zhou, B. B. Jiang, J. D. Wang, Z. W. Liao, Z. L. Huang, Y. R. Yang, *Mol. Catal.* **2019**, *475*, 110493.
[6] a) M. H. Groothaert, P. J. Smeets, B. F. Sels, P. A. Jacobs, R. A. Schoonheydt, *J. Am. Chem. Soc.* **2005**, *127*, 1394–1395; b) J. S. Woertink, P. J. Smeets, M. H. Groothaert, M. A. Vance, B. F. Sels, R. A. Schoonheydt, E. I. Solomon, *Proc. Natl. Acad. Sci. USA* **2009**, *106*, 18908–18913; c) S. Grundner, M. A. C. Markovits, G. Li, M. Tromp, E. A. Pidko, E. J. M. Hensen, A. Jentys, M. Sanchez-Sanchez, J. A. Lercher, *Nat. Commun.* **2015**, *6*, 7546; d) K. Narsimhan, K. Iyoki, K. Dinh, Y. Román-Leshkov, *ACS Cent. Sci.* **2016**, *2*, 424–429; e) G. Li, P. Vassilev, M. Sanchez-Sanchez, J. A. Lercher, E. J. M. Hensen, E. A. Pidko, *J. Catal.* **2016**, *338*, 305–312; f) A. R. Kulkarni, Z.-J. Zhao, S. Siahrostami, J. K. Nørskov, F. Studt, *ACS Catal.* **2016**, *6*, 6531–6536; g) V. L. Sushkevich, D. Palagin, M. Ranocchiari, J. A. van Bokhoven, *Science* **2017**, *356*, 523–527; h) M. H. Mahyuddin, A. Staykov, Y. Shiota, M. Miyanishi, K. Yoshizawa, *ACS Catal.* **2017**, *7*, 3741–3751; i) D. K. Pappas, E. Borfecchia, M. Dyballa, I. A. Pankin, K. A. Lomachenko, A. Martini, M. Signorile, S. Teketel, B. Arstad, G. Berlier, C. Lamberti, S. Bordiga, U. Olsbye, K. P. Lillerud, S. Svelle, P. Beato, *J. Am. Chem. Soc.* **2017**, *139*, 14961–14975; j) G. Wang, W. Chen, L. Huang, Z. Liu, X. Sun, A. Zheng, *Catal. Today* **2019**, *338*, 108–116; k) M. Dyballa, K. Thorshaug, D. K. Pappas, E. Borfecchia, K. Kvande, S. Bordiga, G. Berlier, A. Lazzarini, U. Olsbye, P. Beato, S. Svelle, B. Arstad, *ChemCatChem* **2019**, *11*, 5022–5026; l) A. A. Kolganov, A. A. Gabrienko, S. A. Yashnik, E. A. Pidko, A. G. Stepanov, *J. Phys. Chem. C* **2020**, *124*, 6242–6252; m) A. A. Gabrienko, S. A. Yashnik, A. A. Kolganov, A. M. Sheveleva, S. S. Arzumanov, M. V. Fedin, F. Tuna, A. G. Stepanov, *Inorg. Chem.* **2020**, *59*, 2037–2050; n) A. A. Gabrienko, A. A. Kolganov, S. S. Arzumanov, S. A. Yashnik, V. V. Kriventsov, D. Freude, A. G. Stepanov, *J. Phys. Chem. C* **2021**, *125*, 2182–2193; o) W. Nunthakitgoson, A. Thivasasith, T. Maihom, C. Wattanakit, *Phys. Chem. Chem. Phys.* **2021**, *23*, 2500–2510; p) A. A. Kolganov, A. A. Gabrienko, A. G. Stepanov, *Chem. Phys. Lett.* **2023**, *810*, 140188.
[7] a) R. S. Hanson, T. E. Hanson, *Microbiol. Rev.* **1996**, *60*, 439–471; b) A. S. Hakemian, A. C. Rosenzweig, *Annu. Rev. Biochem.* **2007**, *76*, 223–241.
[8] O. P. Krivoruchko, V. F. Anufrienko, E. A. Paukshtis, T. V. Larina, E. B. Burgina, S. A. Yashnik, Z. R. Ismagilov, V. N. Parmon, *Dokl. Phys. Chem.* **2004**, *398*, 226–230.
[9] a) Z. R. Ismagilov, S. A. Yashnik, V. F. Anufrienko, T. V. Larina, N. T. Vasenin, N. N. Bulgakov, S. V. Vosel, L. T. Tsykoza, *Appl. Surf. Sci.* **2004**, *226*, 88–93; b) S. A. Yashnik, A. V. Salnikov, N. T. Vasenin, V. F. Anufrienko, Z. R. Ismagilov, *Catal. Today* **2012**, *197*, 214–227.
[10] V. F. Anufrienko, S. A. Yashnik, N. N. Bulgakov, T. V. Larina, N. T. Vasenin, Z. R. Ismagilov, *Dokl. Phys. Chem.* **2003**, *392*, 207–211.
[11] A. R. Kulkarni, Z. J. Zhao, S. Siahrostami, J. K. Norskov, F. Studt, *Catal. Sci. Technol.* **2018**, *8*, 114–123.
[12] a) M. A. Newton, A. J. Knorpp, V. L. Sushkevich, D. Palagin, J. A. van Bokhoven, *Chem. Soc. Rev.* **2020**, *49*, 1449–1486; b) Z. R. Jovanovic, J.-P. Lange, M. Ravi, A. J. Knorpp, V. L. Sushkevich, M. A. Newton, D. Palagin, J. A. van Bokhoven, *J. Catal.* **2020**, *385*, 238–245; c) M. H. Mahyuddin, Y. Shiota, K. Yoshizawa, *Catal. Sci. Technol.* **2019**, *9*, 1744–1768.
[13] M. H. Mahyuddin, T. Tanaka, A. Staykov, Y. Shiota, K. Yoshizawa, *Inorg. Chem.* **2018**, *57*, 10146–10152.

[14] D. Zagorac, H. Müller, S. Ruehl, J. Zagorac, S. Rehme; 2019; ICSD Collection Codes: 43493, 64699 for Cu0, ICSD Database (accessed July 28, 2020); DOI: 10.1107/S160057671900997X.
[15] D. Zagorac, H. Müller, S. Ruehl, J. Zagorac, S. Rehme; 2019; ICSD Collection Codes: 69758, 75473 for CuO, ICSD Database (accessed July 28, 2020); DOI: 10.1107/S160057671900997X.
[16] M. A. C. Markovits, A. Jentys, M. Tromp, M. Sanchez-Sanchez, J. A. Lercher, *Top. Catal.* **2016**, *59*, 1554–1563.
[17] C. Baerlocher, L. B. McCusker, R. M. Hanson, Database of Zeolite Structures. http://www.iza-structure.org/databases/ (accessed Oct 10, 2019).
[18] a) G. Turnes Palomino, P. Fisicaro, S. Bordiga, A. Zecchina, E. Giamello, C. Lamberti, *J. Phys. Chem. B* **2000**, *104*, 4064–4073; b) Y. Kuroda, Y. Yoshikawa, S.-i. Konno, H. Hamano, H. Maeda, R. Kumashiro, M. Nagao, *J. Phys. Chem.* **1995**, *99*, 10621–10628.
[19] I. Persson, P. Persson, M. Sandström, A.-S. Ullström, *J. Chem. Soc., Dalton Trans.* **2002**, 7, 1256–1265.
[20] A. B. P. Lever, *Inorganic Electronic Spectroscopy, Vol. 2*, Elsevier, Amsterdam **1984**.
[21] S. A. Yashnik, Z. R. Ismagilov, V. F. Anufrienko, *Catal. Today* **2005**, *110*, 310–322.
[22] F. Giordanino, P. N. R. Vennestrøm, L. F. Lundegaard, F. N. Stappen, S. Mossin, P. Beato, S. Bordiga, C. Lamberti, *Dalton Trans.* **2013**, *42*, 12741–12761.
[23] a) Y. Teraoka, C. Tai, H. Ogawa, H. Furukawa, S. Kagawa, *Appl. Catal. A-Gen.* **2000**, *200*, 167–176; b) S.-K. Park, V. Kurshev, Z. Luan, C. Wee Lee, L. Kevan, *Microporous Mesoporous Mater.* **2000**, *38*, 255–266.
[24] a) M. H. Groothaert, K. Pierloot, A. Delabie, R. A. Schoonheydt, *Phys. Chem. Chem. Phys.* **2003**, *5*, 2135–2144; b) C. E. Sass, L. Kevan, *J. Phys. Chem.* **1988**, *92*, 5192–5196.
[25] a) S. Yashnik, Z. Ismagilov, *Appl. Catal. B-Environ.* **2015**, *170–171*, 241–254; b) P. J. Carl, S. C. Larsen, *J. Phys. Chem. B* **2000**, *104*, 6568–6575; c) A. B. Ene, M. Bauer, T. Archipov, E. Roduner, *Phys. Chem. Chem. Phys.* **2010**, *12*, 6520–6531.
[26] V. A. Matyshak, A. N. Il'ichev, A. A. Ukharsky, V. N. Korchak, *J. Catal.* **1997**, *171*, 245–254.
[27] P. H. Kasai, R. J. Bishop, Jr., *J. Phys. Chem.* **1977**, *81*, 1527–1529.
[28] a) P. Vanelderen, R. G. Hadt, P. J. Smeets, E. I. Solomon, R. A. Schoonheydt, B. F. Sels, *J. Catal.* **2011**, *284*, 157–164; b) S. C. Larsen, A. Aylor, A. T. Bell, J. A. Reimer, *J. Phys. Chem.* **1994**, *98*, 11533–11540; c) A. V. Kucherov, H. G. Karge, R. Schlögl, *Microporous Mesoporous Mater.* **1998**, *25*, 7–14; d) M. Lo Jacono, G. Fierro, R. Dragone, X. Feng, J. d'Itr, W. K. Hall, *J. Phys. Chem. B* **1997**, *101*, 1979–1984; e) A. Godiksen, F. N. Stappen, P. N. R. Vennestrøm, F. Giordanino, S. B. Rasmussen, L. F. Lundegaard, S. Mossin, *J. Phys. Chem. C* **2014**, *118*, 23126–23138.
[29] A. A. Kolganov, A. A. Gabrienko, I. Y. Chernyshov, A. G. Stepanov, E. A. Pidko, *Phys. Chem. Chem. Phys.* **2020**, *22*, 24004–24013.
[30] B. D. Montejo-Valencia, Y. J. Pagan-Torres, M. M. Martinez-Inesta, M. C. Curet-Arana, *ACS Catal.* **2017**, *7*, 6719–6728.
[31] a) M. V. Frash, R. A. van Santen, *Phys. Chem. Chem. Phys.* **2000**, *2*, 1085–1089; b) V. B. Kazansky, A. I. Serykh, E. A. Pidko, *J. Catal.* **2004**, *225*, 369–373; c) M. V. Luzgin, V. A. Rogov, S. S. Arzumanov, A. V. Toktarev, A. G. Stepanov, V. N. Parmon, *Angew. Chem. Int. Ed.* **2008**, *47*, 4559–4562; d) Y. G. Kolyagin, I. I. Ivanova, V. V. Ordomsky, A. Gedeon, Y. A. Pirogov, *J. Phys. Chem. C* **2008**, *112*, 20065–20069; e) A. A. Gabrienko, S. S. Arzumanov, M. V. Luzgin, A. G. Stepanov, V. N. Parmon, *J. Phys. Chem. C* **2015**, *119*, 24910–24918; f) A. Oda, H. Torigoe, A. Itadani, T. Ohkubo, T. Yumura, H. Kobayashi, Y. Kuroda, *J. Phys. Chem. C* **2013**, *117*, 19525–19534; g) M. V. Luzgin, A. A. Gabrienko, V. A. Rogov, A. V. Toktarev, V. N. Parmon, A. G. Stepanov, *J. Phys. Chem. C* **2010**, *114*, 21555–21561; h) A. A. Gabrienko, S. S. Arzumanov, I. B. Moroz, I. P. Prosvirin, A. V. Toktarev, W. Wang, A. G. Stepanov, *J. Phys. Chem. C* **2014**, *118*, 8034–8043.
[32] E. Breitmaier, W. Voelter, *Carbon-13 NMR Spectroscopy: High-Resolution Methods and Applications in Organic and Biochemistry*, third ed., VCH, New York **1990**, p. 530.
[33] a) A. A. Gabrienko, I. G. Danilova, S. S. Arzumanov, L. V. Pirutko, D. Freude, A. G. Stepanov, *J. Phys. Chem. C* **2018**, *122*, 25386–25395; b) M. Hunger, *Solid State Nucl. Magn. Reson.* **1996**, *6*, 1–29; c) D. Freude, *Chem. Phys. Lett.* **1995**, *235*, 69–75.
[34] P. Tomkins, M. Ranocchiari, J. A. van Bokhoven, *Accounts Chem. Res.* **2017**, *50*, 418–425.
[35] M. A. Artsiusheuski, R. Verel, J. A. van Bokhoven, V. L. Sushkevich, *ACS Catal.* **2023**, *13*, 5864–5875.
[36] a) J.-P. Lange, V. L. Sushkevich, A. J. Knorpp, J. A. van Bo, khoven, *Ind. Eng. Chem. Res.* **2019**, *58*, 8674–8680; b) P. J. Smeets, R. G. Hadt, J. S. Woertink, P. Vanelderen, R. A. Schoonheydt, B. F. Sels, E. I. Solomon, *J. Am. Chem. Soc.* **2010**, *132*, 14736–14738.
[37] a) J. A. Labinger, *Science* **2018**, *359*, 4968; b) R. A. Periana, *Science* **2017**, *358*, 5970; c) A. J. Heyer, J. Ma, D. Plessers, A. Braun, M. L. Bols, H. M. Rhoda, R. A. Schoonheydt, B. F. Sels, E. I. Solomon, *J. Am. Chem. Soc.* **2024**, *146*, 21208–21213.
[38] S. A. Yashnik, Z. R. Ismagilov, *Kinet. Catal.* **2016**, *57*, 776–796.
[39] R. K. Harris, E. D. Becker, S. M. C. De Menezes, R. Goodfellow, P. Granger, *Solid State Nucl. Magn. Reson.* **2002**, *22*, 458–483.
[40] C. R. Morcombe, K. W. Zilm, *J. Magn. Reson.* **2003**, *162*, 479–486.
[41] F. Neese, F. Wennmohs, U. Becker, C. Riplinger, *J. Chem. Phys.* **2020**, *152*, 224108.
[42] J. P. Perdew, K. Burke, Y. Wang, *Phys. Rev. B* **1996**, *54*, 16533–16539.
[43] a) S. Grimme, S. Ehrlich, L. Goerigk, *J. Comput. Chem.* **2011**, *32*, 1456–1465; b) S. Grimme, J. Antony, S. Ehrlich, H. Krieg, *J. Chem. Phys.* **2010**, *132*, 154104.
[44] a) W. J. Hehre, R. Ditchfield, J. A. Pople, *J. Chem. Phys.* **1972**, *56*, 2257–2261; b) M. M. Francl, W. J. Pietro, W. J. Hehre, J. S. Binkley, M. S. Gordon, D. J. DeFrees, J. A. Pople, *J. Chem. Phys.* **1982**, *77*, 3654–3665; c) V. A. Rassolov, J. A. Pople, M. A. Ratner, T. L. Windus, *J. Chem. Phys.* **1998**, *109*, 1223–1229.
[45] a) F. Weigend, *Phys. Chem. Chem. Phys.* **2006**, *8*, 1057–1065; b) F. Weigend, R. Ahlrichs, *Phys. Chem. Chem. Phys.* **2005**, *7*, 3297–3305.
[46] G. Henkelman, B. P. Uberuaga, H. Jonsson, *J. Chem. Phys.* **2000**, *113*, 9901–9904.
[47] P. A. Piminov, G. N. Baranov, A. V. Bogomyagkov, D. E. Berkaev, V. M. Borin, V. L. Dorokhov, S. E. Karnaev, V. A. Kiselev, E. B. Levichev, O. I. Meshkov, S. I. Mishnev, S. A. Nikitin, I. B. Nikolaev, S. V. Sinyatkin, P. D. Vobly, K. V. Zolotarev, A. N. Zhuravlev, *Physcs. Proc.* **2016**, *84*, 19–26.
[48] K. V. Klementev, *J. Phys. D: Appl. Phys.* **2001**, *34*, 209–217.
[49] N. Binsted, J. V. Campbell, S. J. Gurman, P. C. Stephenson, EXCURV92, Program for simulating EXAFS spectra, SERC Daresbury Laboratory, Daresbury (England) **1991**.
[50] a) V. L. Sushkevich, R. Verel, J. A. Bokhoven, *Angew. Chem. Int. Ed.* **2020**, *132*, 920–928; b) M. C. Biesinger, *Surf. Interface Anal.* **2017**, *49*, 1325–1334; c) I. Khalakhan, M. Vorokhta, X. Xie, L. Piliai, I. Matolínová, *J. Electron. Spectrosc.* **2021**, *246*, 147027; d) J. P. Espinós, J. Morales, A. Barranco, A. Caballero, J. P. Holgado, A. R. González-Elipe, *J. Phys. Chem. B* **2002**, *106*, 6921–6929.

Manuscript received: August 23, 2024
Accepted manuscript online: January 8, 2025
Version of record online: January 16, 2025